iScience, Volume *23*

Supplemental Information

Divergent Transcription of the *Nkx2-5* Locus Generates Two Enhancer RNAs with Opposing Functions

Irene Salamon, Simone Serio, Simona Bianco, Christina Pagiatakis, Silvia Crasto, Andrea M. Chiariello, Mattia Conte, Paola Cattaneo, Luca Fiorillo, Arianna Felicetta, Elisa di Pasquale, Paolo Kunderfranco, Mario Nicodemi, Roberto Papait, and Gianluigi Condorelli

SUPPLEMENTAL INFORMATION

SUPPELEMENTAL FIGURES

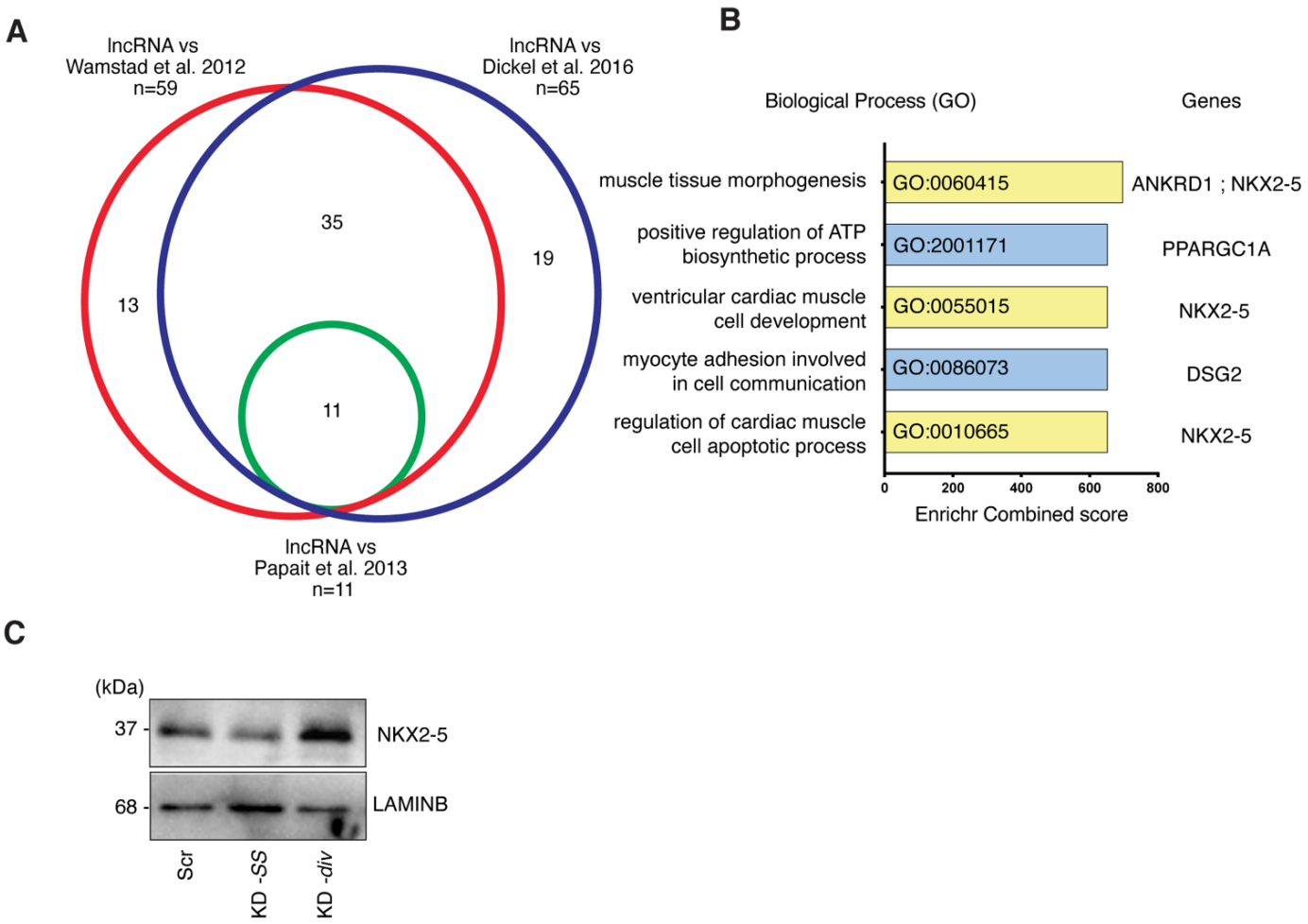

Figure S1. Identification of *IRENE*-SS and *IRENE*-div Upstream of *Nkx2-5*, Related to Figure 1

(A) Venn diagram of the overlap between the identified lncRNAs and three enhancer datasets (Papait et al., 2013a; Wamstad et al., 2012; Dickel et al., 2016).

(B) Enriched biological processes obtained through gene ontology (GO) analysis of the 26 protein-coding genes associated with 46 putative eRNAs. *NKX2-5* is associated with muscle tissue morphogenesis, ventricular cardiac muscle cell development, and regulation of cardiac muscle cell apoptotic processes.

(C) Western blot showing downregulation of NKX2-5 after knockdown (KD) of *IRENE-SS*. Cells were collected 48 h after gapmeR transfection. Scr, scrambled gapmeR; KD-*SS*, gapmeR targeting *IRENE-SS*; KD-*div*, gapmeR targeting *IRENE-div*.

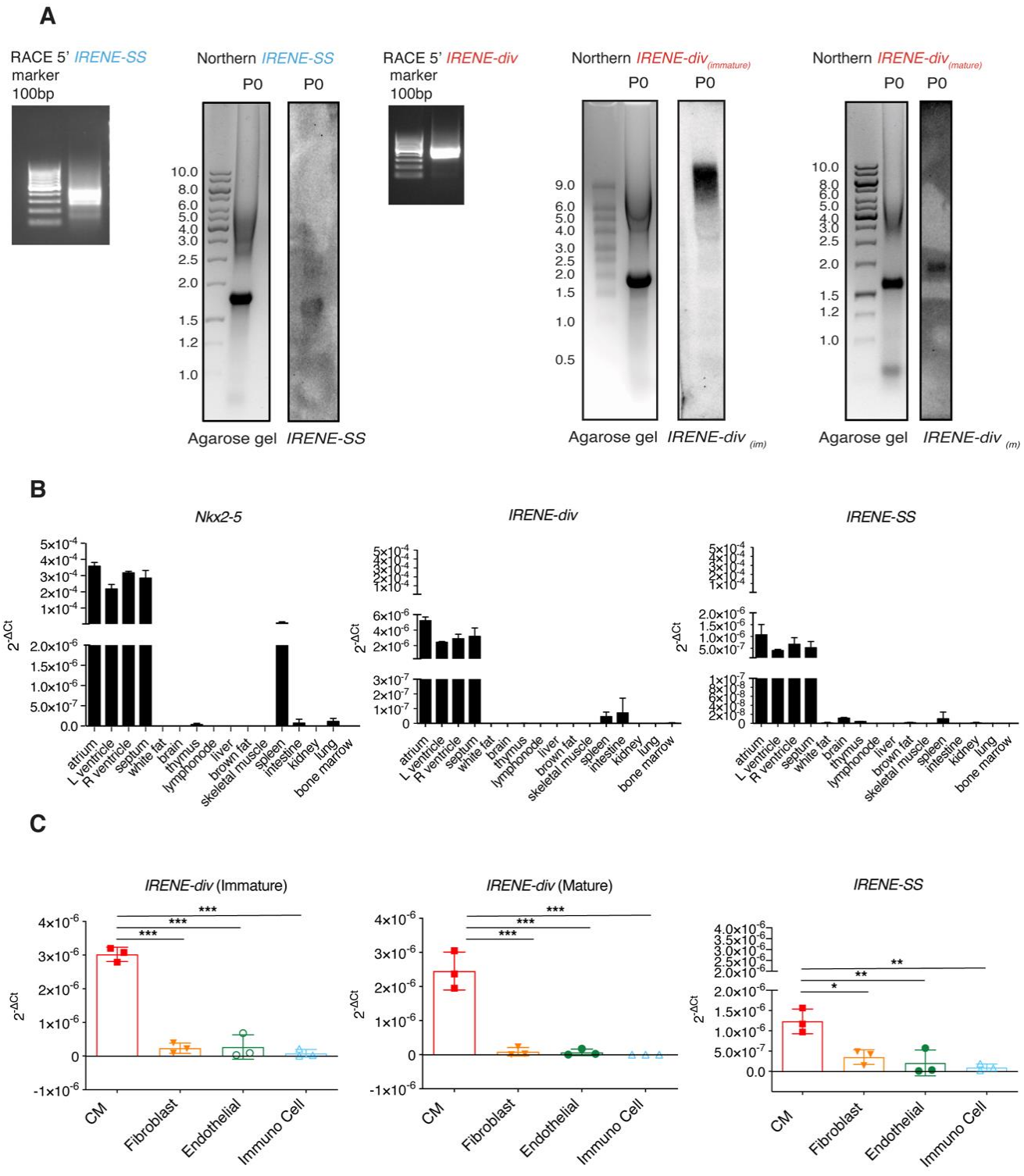

Figure S2. Characterization of *IRENE*-SS and *IRENE*-div Upstream of *Nkx2-5* in Mice, Related to Figure 1

(A) 5' RACE product and Northern blotting for *IRENE-SS* and *IRENE-div*, the latter in its two forms (immature/unspliced and mature).

(B) qRT-PCR analysis of *Nkx2-5*, *IRENE-div*, and *IRENE-SS* in 13 different mouse tissues revealed enrichment in four different cardiac districts.

(C) *IRENE* transcript expression in sorted adult heart cell populations (cardiomyocytes, fibroblasts, endothelia and immune cells), revealing cardiomyocyte-specific enrichment. CM, cardiomyocyte.

Data represented as mean ± SD. *, P-value <0.05; **, P-value <0.01; ***, P-value <0.001.

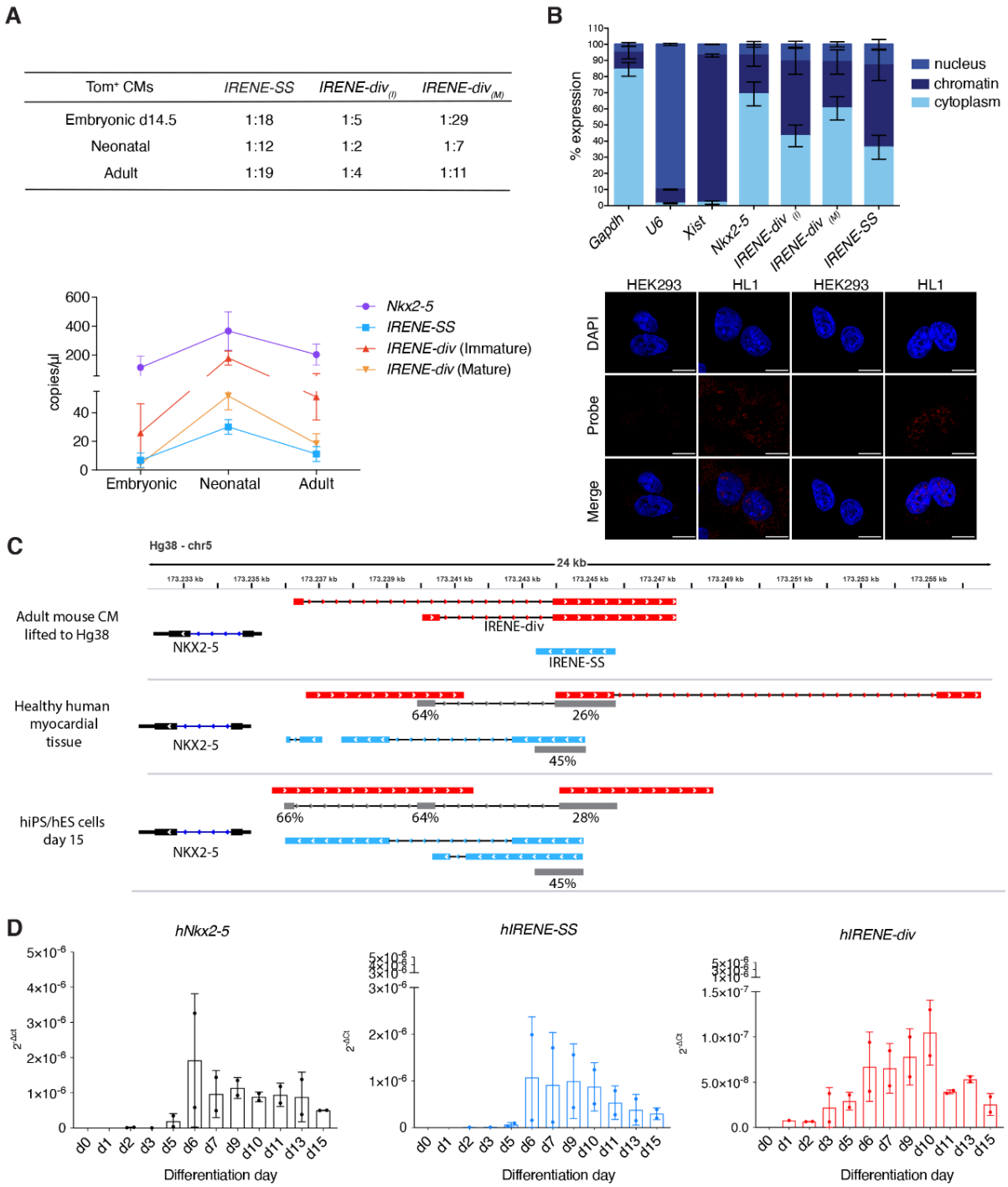

Figure S3. Expression of *IRENE-SS* and IRENE-*div* Upstream of *Nkx2-5* in Mice and Humans, Related to Figure 1

(A) Expression of *Nkx2-5* and *IRENE* transcripts measured by ddPCR at 3 different cardiomyocyte maturation stages: embryonic day 14.5, neonatal day p1, and 8-week-old adult mice. The table indicates the ratio between the copies of *IRENE* and the nearby gene (*Nkx2-5*) at the three different stages, and the graph shows expression reported as copies/µl.

(B) HL1 cell fractionation (nucleus, chromatin, and cytoplasm, as indicated by the different shades) (top) and RNA-FISH (bottom) assessing intracellular localization of *IRENE* transcripts: *IRENE-SS* and immature *IRENE-div* were 60% in the nucleus and mostly chromatin bound, whereas mature *IRENE-div* was 60% in the cytoplasm. *Gapdh*, *U6*, and *Xist* were used as RNA controls for the 3 different compartments. Bars = 10 µm.

(C) Transcript-Transcript Identity scores showing the percentages of identity between mouse and human transcripts.

(D) *Nkx2-5*, *IRENE-SS*, and *IRENE-div* expression in human iPSCs at 12 different time points during cardiomyocyte differentiation (N=2).

Data represented as mean ± SD.

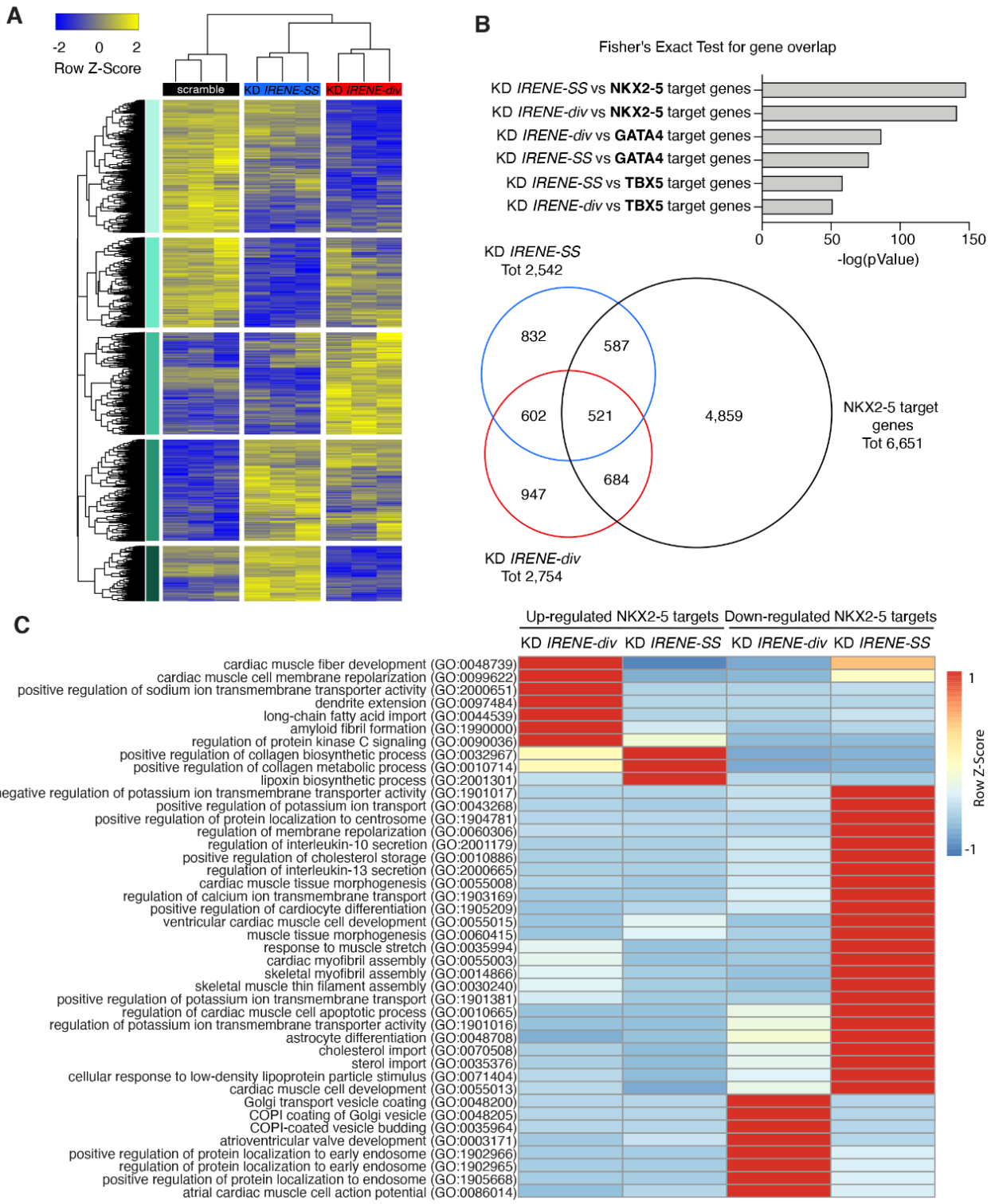

Figure S4. Differential Regulation of *Nkx2-5* by *IRENE-SS* and *IRENE-div*, Related to Figure 1

(A) Heatmap of differentially expressed genes for each gapmeR treatment (FDR ≤0.1; log CPM ≥0).

(B) Bar chart of significant overlaps between genes associated with three TFs (NKX2-5, GATA4, and TBX5) and those modulated upon knockdown of either *IRENE-SS* or *IRENE-div*. Many more modulated genes were targets of NKX2-5 rather than of the other two TFs evaluated. The Venn diagram gives the number of modulated genes that were NKX2-5 targets.

(C) Enriched biological process gene ontology (GO) terms for genes up- and down-regulated by silencing *IRENE-SS* or *IRENE-div*, respectively. The analysis reveals that highlighted terms are oppositely regulated by the silencing of *IRENE-SS* or *IRENE-div*, confirming the opposing effects mediated by the two eRNAs on NKX2-5 target genes.

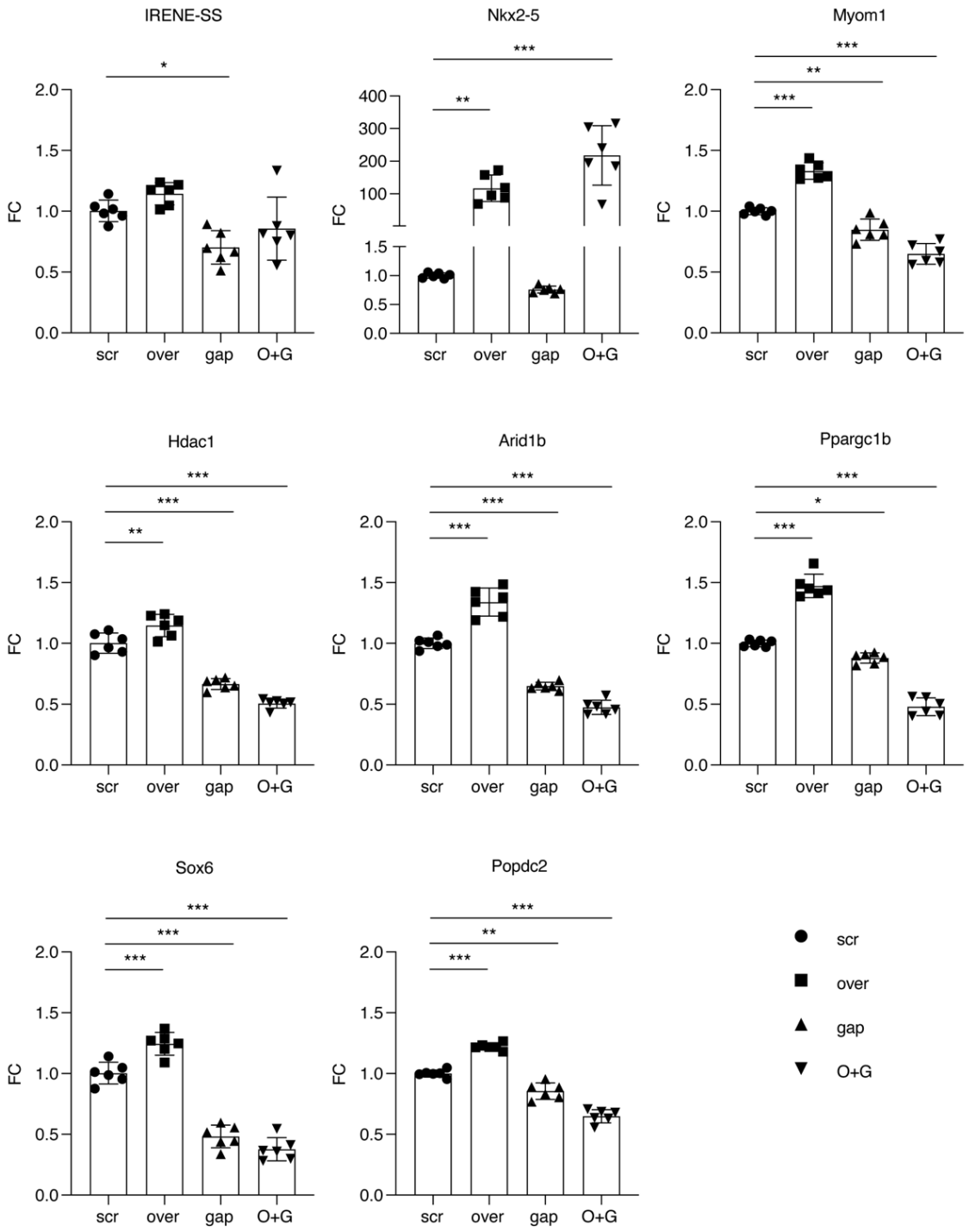

Figure S5. *IRENE-SS* Acts on NKX2-5 Target Genes Independently of NKX2-5 Level, Related to Figure 1

For the six NKX2-5 target genes analysed, overexpression of NKX2-5 increased expression, whereas knockdown of *IRENE-SS* caused a decrease. However, the overexpression of NKX2-5 in neonatal cardiomyocytes with knocked-down *IRENE-SS* did not restore correct expression of the genes. Scr, scramble-treated cells (transfected with a control vector and the control gapmeR); over, cells treated with an NKX2-5 overexpression vector; gap, cells treated with gapmeR targeting *IRENE-SS;* O+G, cells treated with the combination of overexpression vector and gapmeR targeting *IRENE-SS.*

Data represented as mean ± SD. *, P-value <0.05; **, P-value <0.01; ***, P-value <0.001 (one-way ANOVA with Sidak post hoc test).

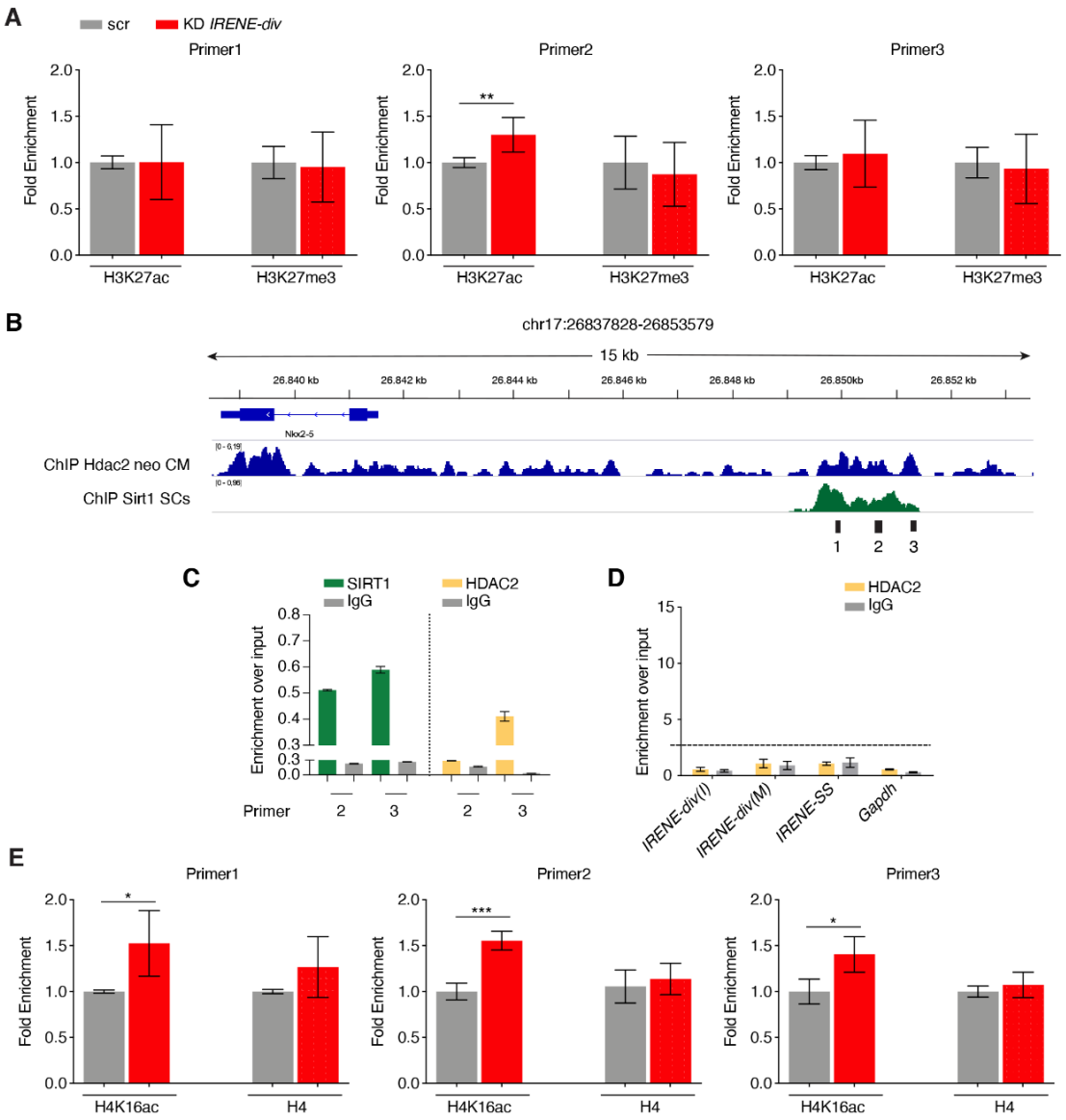

Figure S6. *IRENE-div* Recruits Histone Deacetylase to the *Nkx2-5* Enhancer and its Reduced Impact on Acetylation Status, Related to Figure 3

(A) ChIP−qRT-PCR conducted on neonatal cardiomyocytes revealed an enrichment of H3K27ac on the enhancer region (significant with primer 2) upon *IRENE-div* silencing, with no effect on methylation (H3K27me3). Values are expressed as fold enrichment on scr-treated cells. N=3 biological replicates.

(B) Cardiomyocyte ChIP-seq tracks of HDAC2 and SIRT1 from published datasets on neonatal CMs (neo CM) and skeletal muscle satellite cells (SCs) (Ai et al., 2017; Plimpton, 1995), showing peaks at the enhancer locus.

(C) Validation of ChIP-seq peaks from published datasets of two deacetylases − SIRT1 (green) and HDAC2 (yellow) − through ChIP−qRT-PCR performed on HL1 cells using primers 2 and 3 on the enhancer element.

(D) RIP performed on HL1 cells, using antibodies against HDAC2, showing that immature and mature forms of *IRENE-div* do not bind HDAC2. Interaction is expressed as enrichment over input in N=3 different experiments (one-way ANOVA with Sidak post hoc test). I, immature form; M, mature form.

(E) ChIP−qRT-PCR conducted on neonatal cardiomyocytes after silencing of *IRENE-div* (red bar) compared with scrambled gapmeR-treated cells (grey bar). We used the antibodies against H4K16ac and H4, and three primers (1, 2, and 3) designed on genomic enhancer elements. Knockdown of *IRENE-div* led to a decrease in the enrichment of SIRT1 and a consequential increase in H4K16ac, the histone modification mark induced by SIRT1, whereas no change was detected in the control (H4 immunoprecipitation). Values are expressed as fold enrichment over scr-treated cells. N=2 biological replicates (Student's unpaired t-test).

Data represented as mean ± SD. *, P-value <0.05; **, P-value <0.01; ***, P-value <0.001.

TRANSPARENT METHODS

Annotation, Identification, and Conservation of lncRNAs and eRNAs

Adult mouse cardiomyocyte RNA-seq data (from GSE66847 and GSE96690), human RUES2 cells, iPSC-derived CMs at day 15 of differentiation, and myocardial tissue from nine healthy humans (from GSE130036) were mapped using HISAT2 (Kim et al., 2019) and aligned against GRCm38 and GRCh38 for mouse and human samples, respectively. BAM files with aligned paired-end reads were split into two strand-specific BAM files using SAMtools (Li et al., 2009). The properly paired reads originating from each strand were selected using SAM Flags 99 and 147 for one strand, 83 and 163 for the other strand. Forward (Fw) and reverse (Rw) strand was assigned according to the dUTP method used for sequencing. The transcript assembly was performed on each strand-specific BAM file, using StringTie (Pertea et al., 2015) with parameters -s 2 -g 100 for lncRNA identification. The potential transcripts identified were unified using StringTie –merge with parameters -T 0 -F 0, according to each set of replicated biological data. Transcripts with FPKM <0.1 were subsequently excluded using FPKM_count.py module from RSeQC software (Wang et al., 2012). Slncky (Chen et al., 2016), with default parameters, was used to predict the orthologous transcripts in human samples (hiPSC-derived CMs and healthy human myocardial tissue). Only orthologues identified in both datasets were considered. Three published enhancer datasets (Papait et al., 2013a; Wamstad et al., 2012; Dickel et al., 2016) were used to select the putative eRNAs, identified as lncRNAs that overlapped with enhancer genomic regions. The overlap between genomic regions was performed with IntersectBed (Quinlan and Hall, 2010). The list of 26 protein-coding genes associated with the eRNAs was then analysed using the online tool Enrichr (Kuleshov et al., 2016) to identify GO enrichments. The presented combined score (c) represents the multiplication of the p-value (Fisher exact test) and the z-score (z) of the deviation from the expected rank ($c=\log(p)\cdot z$; for more details, see: http://amp.pharm.mssm.edu/Enrichr/.

Mouse RNA-sequencing

Three biological replicates of neonatal primary CM cultures for each specific gapmeR treatment were profiled. DNase I-treated RNA analysed on the Tape Station 4200 (Agilent) showed an RNA integrity number (RIN) of 9.7−9.8. SMART-seq v4 Ultra Low Input RNA Kits (Takara Bio) were used for cDNA amplification. Indexed sequencing libraries were generated using Nextera XT DNA Library Preparation Kits (Illumina) following the manufacturer's instructions. Electrophoresis of the libraries on a LabChip GX instrument showed average library size of 500−555 bp. Single-end multiplexed libraries were sequenced using a NextSeq500 instrument. 19−34 million reads/sample were obtained. Single-end reads of 75 bp were aligned to the GENCODE *Mus musculus* reference genome (build GRCm38/mm10) using STAR v2.7.2b (Dobin et al., 2013). Raw read counts were normalized with TMM implemented in edgeR (Robinson et al., 2010); differential expression analysis of read counts was performed using glmQLFit and glmQLFTest functions. Significant differential genes were chosen based on an FDR ≤0.1 and logCPM ≥0. Hierarchical clustering of significantly modulated genes was performed using hclust and dist R functions (R Core Team, 2019). Clustering was performed with complete linkage method and Euclidean distance to generate a heatmap using pheatmap (Kolde, 2019).

Human RNA-sequencing

One biological replicate of human RUES2 cells and one of iPSC-derived CMs at day 15 of differentiation were profiled. DNase I-treated RNA analysed on the LabChip GXT (PerkinElmer) had RIN >7. Indexed sequencing libraries were generated using TruSeq Stranded Total RNA LT with Ribo-Zero Human/Mouse/Rat (Illumina), following the manufacturer's instructions. Electrophoresis of the libraries on a LabChip GXT instrument showed an average library size of 311bp. Paired-end multiplexed libraries were sequenced using the NextSeq500 instrument. 96−104 million reads for each sample were obtained.

Nkx2-5, *Tbx5*, and *Gata4* Gene Analysis

Nkx2-5, *Tbx5*, and *Gata4* average footprints obtained from *in vitro* differentiated mouse CMs (GSE72223) were used. Only ChIP-seq peaks that fell on gene promoters (−3kb/+2kb from the TSS) and/or enhancer genomic regions were selected. The NKX2-5, TBX5, and GATA4 target gene sets were identified using rGreat (Gu, 2019), using "oneClosest" rule and "adv_oneDistance = 500" to associate the selected regions to the nearby gene. Fisher test R function was used to test the significant overlap between modulated genes obtained from RNA-seq of the *IRENE-SS* and *IRENE-div* knockdown and the TF's associated targets identified. GO enrichment analysis was performed with enrichR (Jawaid, 2019) and, using pheatmap, we plotted the raw z-score computed by centring and scaling the "enrichR combined scores". RNA-seq data has been deposited in the NCBI GEO database (GSE143930, GSE143929).

Primary Cardiomyocyte Culture

Primary CMs were isolated from 1-day-old pups with the Neonatal Heart Dissociation Kit (Miltenyi). Cells were cultured in M-199, DMEM, 1% penicillin/streptomycin (Pen-Strep, 10000 U/ml), 1% ultraglutamine, 10% horse serum, and 5% foetal bovine serum (FBS).

HL1 Cell Culture
HL-1 cells, a mouse atrial CM immortalized cell line, were grown in Claycomb Medium (Sigma-Aldrich) supplemented with 10% FBS (Sigma-Aldrich), 1% Pen-Strep, 1% ultraglutamine (200 mM), and 1 mM norepinephrine (Sigma-Aldrich) on gelatin/fibronectin pre-coated flasks. After reaching full confluence, cells were split according to Dr. Claycomb's instructions (Claycomb et al., 1998).

GapmeR Silencing and NKX2-5 Overexpression
Transfections were carried out using standard Lipofectamine 2000 (ThermoFisher) protocols. GapmeR silencing was performed using 100 nM of scrambled, anti-*IRENE-SS*, or anti-*IRENE-div* sequences (QIAGEN). Cells were harvested after 24 h and 48 h for qRT-PCR, 48 h for Western blotting, and 24 h for ChIP−qRT-PCR. The antisense LNA GapmeR standard sequences were: scr negative control A 5'-3': AACACGTCTATACGC; anti-*IRENE-SS* 5'-3': GAAGGTGATAATTTGA; and anti-*IRENE-div* 5'-3': TTCGGGTCAAGAGTGC.

Overexpression was conducted using 250 ng of Nkx2-5 overexpression pcDNA3 vector. The rescue experiment was performed combining the transfection of 100 nM of gapmeR anti-*IRENE-SS* and 250 ng of overexpression vector in neonatal cardiomyocytes or the same amount of scrambled gapmeR and empty control vector. Cells were collected after 24 h and processing for qRT-PCR.

Human Induced Pluripotent Stem Cell-derived Cardiomyocytes
An erythroid body-based protocol was used to generate functional cardiomyocyte-like cells from feeder-free female and male hiPSCs. Human samples were collected after written informed consent by the patients. The expression of markers typical of pluripotent cells and karyotype was used to control cell lines, as described elsewhere (Di Pasquale et al., 2013). hiPSCs were differentiated using the monolayer differentiation protocol as described elsewhere (Salvarani et al., 2019). In brief, iPSCs were treated with 12 µM CHIR99021 and 5 µM IWR and cultured until they started to spontaneously beat.

The following twelve different stages of hiPSC-CMs differentiation were used for the experiments: days 0, 1, 2, 3, 5, 6, 7, 9, 10, 11, 13, and 15. Two sets of differentiation experiments were used and merged. RNA was extracted, retro-transcribed, and used for qRT-PCR. The primer sequences for the gene expression analyses were:

hNKX2-5: Fw GAGCCGAAAAGAAAGCCTGAA, Rw CACCGACACGTCTCACTCAG;
hIRENE-div: Fw GACATCACCCTCCCATTCCT, Rw AGAGTCATCTCCAGGGCTACC;
hIRENE-SS: Fw GGCAGACCCCACACTTCA, Rw TTCCACGCTTGTTCAGTGC.

Sorting of Pure Cardiomyocytes and Heart Cell Populations
To isolate pure CM populations, we used a constitutively active CM-specific tdTomato reporter mouse (αMHC Cre/$^{+}$;R26tdTomato) that expresses Cre recombinase protein under control of the alpha myosin heavy chain (αMHC) promoter (Abel et al., 1999) in addition to a loxP site-dependent tdTomato reporter within the ubiquitous *Rosa26* gene locus, in the C57BL/6J background (Larcher et al., 2018). Cells were sorted to isolate CMs (Tom^{+}), fibroblasts (CD45^{-}/PDGFα^{+}), endothelial cells (CD45^{-}/CD31^{+}), and leukocytes (CD45^{+}). All experiments were performed according to the 2010/63/EU Directive and approved by the ethics committee of Humanitas Research Hospital.

RNA Preparation
RNA was extracted using PureZOL isolation reagent (BioRad), following the manufacturer's instructions, for mouse tissues, Northern blotting, and RIP. The Zymo Extraction Kit (EuroClone), plus DNAse treatment on columns, was used for RNA-seq, qRT-PCR, and ddPCR.

Quantitative RT-PCR
RNA was retro-transcribed using the High Capacity cDNA Reverse Transcription Kit (Applied Biosystems) for gene expression, and the SuperScript Vilo cDNA Synthesis Kit (Invitrogen) for fractionation and RIP. qRT-PCR was performed using the SYBR Green PCR Master Mix (Applied Biosystems). Primers used were:

IRENE-SS: Fw CGTTTATGCTGTAGCGCTGT, Rw CTTGGGGCTGTGATTGATTT;
IRENE-div (immature): Fw AGCATGAAGGAGCGTGACTT, Rw GTGCAGGTACAGGGGTTGTT;
IRENE-div (mature): Fw AGGACCTTGTTACTGGCACTG, Rw TGTCTGTCTTTCTGTCTGGAGAA.

Hprt was used to normalize Ct values, and the $2^{-\Delta Ct}$ method and fold change were conducted to analyse data.

Droplet Digital PCR
The QX200 ddPCR system (BioRad) and an EvaGreen-based assay were used. The PCR reaction mix was loaded into 96-well plates in an automated droplet generator. The plate was sealed, placed in the thermal cycler, and after the PCR reaction put into the droplet reader, experimental details set using QuantaSoft (BioRad), and the reading started. Data analysis was performed using QuantaSoft and values expressed as copies/µl.

RNA-Fluorescent in-situ hybridization (FISH)

Custom Stellaris FISH probes were designed against *IRENE-SS* and *IRENE-div* by utilizing the Stellaris RNA FISH Probe Designer (Biosearch Technologies) available online at www.biosearchtech.com/stellarisdesigner (version 4.2). HL1 and HEK293 cells were hybridized with the *IRENE-SS* and *IRENE-div* Stellaris RNA-FISH probe set labelled with TAMRA-C9 and QUASAR 670 dye, respectively (Biosearch Technologies), following the manufacturer's instructions available online at www.biosearchtech.com/stellarisprotocols. Briefly, the cells were fixed with 3.7% formaldehyde and permeabilized 1 h at 4°C with 70% ethanol. The coverslips were washed and hybridized overnight at 37°C in Hybridization Buffer with 2µl of specific probe (stock solution: 12.5 µM). The coverslips were then washed, stained with DAPI, and mounted on slides using one drop of FluorSave Reagent (Millipore).

Cell Fractionation

HL1 cells were collected in phosphate-buffered saline (PBS) and lysed in Cytoplasm Buffer (50 mM Tris-HCl [pH 8.0], 140 mM NaCl, 1.5 mM $MgCl_2$, 0.5% NP-40) supplemented with RNAsin (Promega) for 10 min on ice. After centrifugation at 500 rpm for 5 min, the supernatant was collected as the cytoplasmic fraction. The remaining pellet was washed in 1X PBS and resuspended in Nucleoplasm Buffer (50 mM Tris-HCl [pH 8.0], 500 mM NaCl, 1.5 mM $MgCl_2$, 0.5% NP-40) supplemented with RNAsin for 10 min on ice. Chromatin was pelleted at maximum speed for 5 min. Supernatant was collected as the nucleoplasm and the chromatin pelleted in 1X PBS. RNA from cytoplasmic and nucleoplasm fractions were precipitated using $C_2H_3NaO_2$. RNA was extracted using the Zymo Kit supplemented with DNAse. The Super Script VILO cDNA Synthesis Kit (Invitrogen) was used to retro-transcribe RNA, with ddPCR to quantify target genes.

Chromatin Immunoprecipitation

For ChIP−qRT-PCR, cells were crosslinked in 1% formaldehyde and lysed to prepare nuclear extracts. Chromatin was sonicated to an average length of 200–300 bp using a Bioruptor Pico (Diagenode), clarified, precleared for 1 h, and immunoprecipitation performed at 4°C overnight with protein G Dynabeads (Invitrogen) coupled with the following antibodies (2 µg for histone modification, 10 µg for transcription factor and HDAC): anti-H3K27ac (ab4729, Abcam), anti-H3K27me3 (07-449, Millipore), anti-H4 (ab10158, Abcam), anti-H4K16ac (17-10101, Millipore), anti-NKX2-5 (sc-8697, Santa Cruz), anti-SIRT1 (ab12193, Abcam), anti-HDAC2 (ab7029, Abcam). The washes were made in Buffer I (1 mM EDTA, 0.1% SDS, 10 mM Tris HCl [pH 8.0], 140 mM NaCl, 0.1% sodium deoxyxholate, 1% Triton X-100), Buffer II (1 mM EDTA, 0.1% SDS, 10 mM Tris HCl [pH 8.0], 500 mM NaCl, 0.1% sodium deoxyxholate, 1% Triton X-100), Buffer III (1 mM EDTA, 10 mM Tris HCl [pH 8.0], 250 mM LiCl, 0.5% sodium deoxycholate, 0.5% NP-40), and Tris-EDTA (pH 8.0). Crosslinking was reverted overnight in Elution Buffer (5 mM EDTA, 10 mM TrisHCl [pH 8.0], 300 mM NaCl, 0.5% SDS) shaking at 65°C. Proteinase K treatment for 2 h shaking at 45°C. DNA was extract with phenol:chloroform extraction. Primer sequences for ChIP−qRT-PCR were:

ChIP_1: Fw GCCATTCGCTCCTAGCTTC, Rw GGGCAGTGACTCTTGGACTC;
ChIP_2: Fw CCTCGCTCCAGTCAAACTTC, Rw CCACACAGCAGAGGGTTTGT;
ChIP_3: Fw ACTTTGGAAGGGGAGAGGAG, Rw GGAAGTGGAGCAGTTGAAGC;
ChIP_4: Fw TCTCTGCCCTGGATGTGG, Rw CCCCTACTCCAGCCTGCTC;
ChIP_5: Fw CTGTCCTTCGCGTTCCTG, Rw AGTGACCCGCTCCATGTC;
Ctrl: Fw GTAGATGGGATGGGTCATGG, Rw TGCTTTGAGGTTGCTTTGTG.

Western Blotting

Cells were washed with PBS and lysed in NP-40 lysis buffer (50 mM Tris, 150 mM NaCl, 0.5% NP-40, 2 mM EDTA, 100 mM NaF, 10 mM sodium pyrophosphate) containing Protease Inhibitor Cocktail (Roche) and 1 mM phenylmethylsulfonyl fluoride. Protein concentrations were determined by the Bradford assay and 30 µg of total protein was resolved on SDS-PAGE and blotted onto nitrocellulose (BioRad) for 1 h. Non-specific binding sites were blocked using 5% milk in PBS-Tween. Membranes were incubated with primary antibodies overnight at 4°C in 5% bovine serum albumin in PBS. Primary antibodies were: anti-Nkx2-5 (1:500; Santa Cruz), anti-lamin B (1:500; Santa Cruz), anti-tubulin (1:2000, Abcam), and anti-Sirt1 (1:1000, Millipore). Membranes were incubated with the HRP-conjugated secondary antibody (donkey anti-goat-HRP, goat anti-rabbit-HRP, goat anti-mouse-HRP, 1:2000 in 5% milk-PBS-T) for 1 h at room temperature. Protein was detected with Enhanced Chemiluminescence Western Blotting Substrate (Immobilon).

Northern Blotting

RNA was extracted using PureZOL isolation reagent (BioRad) and mixed in a 1:1 ratio with RNA sample loading buffer, boiled for 6 min at 70°C, and run on 1% agarose gel (1X MOPS buffer, 1% formaldehyde) in 1X MOPS buffer at 70 V for 3 h. The gel was subsequently transferred to a positively charged nylon membrane in 20X SSC buffer by standard capillary transfer overnight. RNA was crosslinked to the membrane using UV fixation at 200 mJ for 3 min. Membrane was pre-hybridized in NorthernMax Pre-hybridization/Hybridization Buffer for 3 h at 60°C. Membranes were incubated overnight with DIG-conjugated probes diluted in Hybridization Buffer at 60°C. Membranes were then washed in Northern blot low

stringency buffer (3 times, 10 min/wash) at 60°C, followed by washes in Northern blot high stringency buffer (3 times, 10 min/wash) at 60°C, and one wash in 1X PBS-Tween at room temperature for 5 min. Membranes were blocked in 1% blocking solution in 1X PBS-T (Roche) for 30 min at room temperature and then incubated with α-DIG-HRP secondary antibody (1:2000) for 1 h at room temperature. Membranes were washed 3 times in 1x PBS-Tween at room temperature, and RNA visualized using enhanced chemiluminescence.

RNA Immunoprecipitation

For RIP, HL1 cells were crosslinked using 150 mJ UV irradiation, washed in 1X PBS, scraped, and collected by centrifugation at 1000 rpm for 5 min. The cell pellet was lysed in RIP lysis buffer (25 mM Tris-HCl [pH 7.4], 150 mM KCl, 5 mM EDTA, 0.5% NP-40, 0.5 mM DTT, protease inhibitors, and RNA inhibitor) on ice for 30 min. Lysate was centrifuged at 15,000 rpm for 10 min to remove cell debris, and incubated for 1 h (rotating, 4°C) with 50 µL protein-G magnetic beads (washed 3 times in 1X PBS) for pre-clearing. Pre-cleared lysate was then incubated overnight with previously conjugated antibody-protein-G-bead complexes (beads incubated with 10 µg primary antibody overnight at 4°C, rotating). Bead-antibody-lysate complexes were washed three times in 1X PBS, and RNA eluted with 300 µl PureZOL isolation reagent (BioRad), followed by classical RNA extraction.

RNA Pull-down

RNA pull-down was performed as described elsewhere (Yamazaki et al., 2018). Briefly, a portion of *IRENE-SS* or *IRENE-div* was cloned into the pBlueScript II KS (+) vector, and sense or antisense RNAs were synthetized using MAXIscript (Thermo Fisher Scientific) with T7 or T3 RNA polymerase, respectively, and DNase I. RNAs were precipitated with ammonium acetate/ethanol and subsequently biotinylated using the Pierce RNA 3′ End Biotinylation Kit (Thermo Fisher Scientific). HL1 cell extract (CE) was prepared using Cell Extraction Buffer (Thermo Fisher Scientific) following the manufacturer's instructions. The CE was precleared with 50 µl of Dynabeads M-280 Streptavidin (Thermo Fisher Scientific) washed with RNA Pulldown Buffer (1X PBS, 0.1% Triton X-100, 0.6 mM PMSF, Roche Complete Protease Inhibitor Cocktail) and incubated with rotation at 4°C for 1 h. 1 µg of *in vitro*-transcribed RNAs was heated at 90°C for 2 min and then placed on ice for 2 min. An equal volume (10 µl) of RNA structure buffer (20 mM Tris-HCl [pH 7.4], 0.2 M KCl, 20 mM $MgCl_2$) was added and placed at room temperature for 20 min. RNA was then mixed with washed 50µl Dynabeads M-280–Streptavidin and rotated at 4°C for 1 h. The conjugated beads were then washed five times with cold RNA pulldown buffer and incubated with precleared CE in rotation at 4°C for 3 h. Finally, proteins were eluted at 95°C for 5 min in Laemmli sample buffer and load on SDS-PAGE gels.

Immunofluorescence

Cells were fixed in 4% paraformaldehyde, permeabilized with 0.3% triton in PBS, blocked, and incubated with a primary rabbit polyclonal anti-SIRT1 (Millipore) and mouse monoclonal anti-LAMIN B1 (B10, Santa Cruz), both diluted 1:200, and detected using Alexa Fluor 594- or 647-conjugated secondary antibodies (1:500; Life Technology). Cells were visualized using confocal fluorescence microscopy.

3D Modelling

Strings & Binders modelling of the *Nkx2-5* locus: Three-dimensional (3D) conformations of the *Nkx2-5* locus were reconstructed using the SBS polymer chromatin model (Barbieri et al., 2012), which quantitatively describes the biological scenario where chromatin contacts are mediated by proteins, such as TFs, which can bind multiple chromatin sites simultaneously and, thus, bridge them together. Chromatin filaments are represented as self-avoiding chains of beads, some of which are binding sites for specific, diffusing particles named binders. If the binder concentration c and the bead-binder interaction energy E_{int} are above threshold, stable contacts can be formed and the system undergoes coil-globule phase transition. In general, binding sites can be of different types, each interacting with its specific, cognate binders. Schematically, different binding sites can be visualized as different colours, as shown in Figure 4A. Bead−binder interaction of the same colour drives the folding of the chain. The SBS model for the *Nkx2-5* locus, i.e. the optimal number of different types of binding sites and their arrangement along the polymer, were inferred with the PRISMR learning algorithm (Bianco et al., 2018). Briefly, PRISMR uses as its only input a contact map of the locus of interest, such as Hi-C, and iteratively finds the polymer that minimizes the distance between the input and model contact map. Here, we employed Hi-C data from (Rosa-Garrido et al., 2017) at 5kb resolution to model a 200kb region around the *Nkx2-5* gene (mm10, chr17:26740000-26945000) in mouse CMs. The optimal polymer model inferred by our procedure was made up of 615 beads and included 15 different binding site types (Figure 4D).

Polymer model simulations: An ensemble of equilibrium 3D conformations of our polymer model was generated by massive parallel molecular dynamics (MD) simulations performed with the freely available LAMMPS software (Plimpton, 1995). The SBS polymer is initialized in a self-avoiding walk (SAW) conformation, with binders randomly placed in the surrounding environment. The simulation is performed in a cubic box with linear side as long as at least twice the gyration radius of the polymer SAW conformation. Periodic boundary conditions were implemented to reduce finite size effects. Starting from its

initial conformation, the system (i.e. beads and binders) evolves by Langevin dynamics, with standard interaction potentials described in classical polymer physics studies (Kremer and Grest, 1990) and widely employed in the field (Annunziatella et al., 2018).

The main system parameters are the binder concentration c and binding interaction energy E_{int}. The values for c and E_{int} were set to ensure the coil-globule transition (Chiariello et al., 2016), in order to achieve thermodynamically stable conformations. In particular, we employed c ~0.02% (expressed in volume fraction) and $E_{int} = 8.1K_BT$, in line with previous studies (Barbieri et al., 2017; Chiariello et al., 2016). Starting from the SAW conformations, the system evolved up to $2x10^8$ simulation time-steps, so to reach thermodynamic equilibrium where the polymer is completely folded. The complete ensemble of configurations consists of equilibrium structures obtained from 10^2 independent simulations. Figure 4C shows a typical model conformation of the *Nkx2-5* locus obtained from an MD simulation.

Contact maps and correlation metrics: From the generated ensemble of 3D polymers, we computed the average contact map for the SBS model (Figure 4B) as the probability of contact between each pair of polymer beads i and j, by considering them in contact if their Euclidean distance $r_{i,j}$ was below a threshold (Chiariello et al., 2016). To compare Hi-C and model contact maps of the *Nkx2-5* locus, we employed the Pearson correlation coefficient, r, and the distance-corrected correlation, r' (Bianco et al., 2018). r' is introduced to avoid the trivial contribution of the decaying trend of the contact probability as a function of the genomic distance. It is computed as the Pearson correlation coefficient between experimental and model matrices obtained by replacing each matrix element (i,j) with its relative variation with respect to the average contact probability at the genomic distance |i-j|.

Comparison of the model binding sites tracks with epigenetic marks: To investigate the biological nature of the model's inferred binding sites, we compared them with available ChIP-seq peaks of histone marks (Papait et al., 2013b) and CTCF (Rosa-Garrido et al., 2017). To this aim, we binned the ChIP-seq tracks at 5kb resolution and computed Pearson correlation coefficients between each binding site and epigenetic track pair (Bianco et al., 2018) (Figure 4D). Next, we tested the statistical significance of the obtained correlations by comparing them against a random control model. We built the control model as a distribution of correlations between ChIP-seq data and randomized binding sites tracks (10^3 independent realizations), obtained by bootstrapping the original binding sites positions (Bianco et al., 2018). We considered as significant the correlations falling below the 10^{th} percentile (negative correlations) and above the 90^{th} percentile (positive correlations) of the random control distribution. Resulting significant correlations are given in Figure 4D.

Modelling the impact of the eRNA on folding: To test *in silico* the impact of the eRNAs on 3D folding, we implemented the observed decrease in acetylation after *IRENE-SS* silencing. To this aim, the wild-type (wt) model binding sites which correlate with H3K27ac, i.e. types 7 (light blue) and 9 (purple) of Figure 4D were made inert (i.e. converted in non-interacting, grey beads) in the two 5kb windows containing the eRNAs and the enhancer (chr7:2674105000-2674115000). Next, the model contact matrix was re-computed and compared with the wt Hi-C by measuring distance-corrected correlation r' (silenced). To speed up computation, we used the mean-field approximation of the model contact matrices described in (Bianco et al., 2018). Notably, after silencing we found a significant correlation decrease, $\Delta r' = r'(wt)-r'(silenced)$, in the *Nkx2-5* TAD region (green area in the 3D colour scheme of Figure 4E), statistically higher than the correlation decrease found in a control model built by silencing in turn all other possible bins pairs (105 pairs in total) within the region, excluding bins containing CTCF sites (Figure 4E, empirical P-value $<1/105\approx0.01$). A subtraction map between the silenced and wt model contact matrices (silenced - wt) was also produced to highlight the contact changes around the silenced region (Figure 4F). In particular, the model predicts a reduction of the contact frequency between the gene and enhancer region (dashed box in Figure 4F) of ~30% with respect to the wild type.

Statistical Analysis

Unpaired t-test was used for two-group comparisons, and ordinary one-way ANOVA for multiple comparisons. Statistical analyses were performed with GraphPad Prism 8 software on at least two or three independent experiments, and two-sided P-value calculated (*, $P<0.05$; **, $P<0.01$; ***$P<0.001$). Data are represented as mean ± standard deviation (SD).

SUPPLEMENTAL REFERENCES

Abel, E. D., Kaulbach, H. C., Tian, R., Hopkins, J. C., Duffy, J., Doetschman, T., Minnemann, T., Boers, M. E., Hadro, E., Oberste-Berghaus, C., et al. (1999). Cardiac hypertrophy with preserved contractile function after selective deletion of GLUT4 from the heart. J Clin Invest 104**,** 1703-14.

Annunziatella, C., Chiariello, A. M. a. M., Esposito, A., Bianco, S., Fiorillo, L. and Nicodemi, M. (2018). Molecular Dynamics simulations of the Strings and Binders Switch model of chromatin. Methods 142**,** 81-88.

Barbieri, M., Chotalia, M., Fraser, J., Lavitas, L. M., Dostie, J., Pombo, A. and Nicodemi, M. (2012). Complexity of chromatin folding is captured by the strings and binders switch model. Proc Natl Acad Sci U S A 109**,** 16173-16178.

Barbieri, M., Xie, S. Q., Torlai Triglia, E., Chiariello, A. M., Bianco, S., De Santiago, I., Branco, M. R., Rueda, D., Nicodemi, M. and Pombo, A. (2017). Active and poised promoter states drive folding of the extended HoxB locus in mouse embryonic stem cells. Nat Struct Mol Biol 24**,** 515-524.

Chiariello, A. M., Annunziatella, C., Bianco, S., Esposito, A. and Nicodemi, M. (2016). Polymer physics of chromosome large-scale 3D organisation. Sci Rep 11**,** 559.

Claycomb, W. C., Lanson, N. A., Jr., Stallworth, B. S., Egeland, D. B., Delcarpio, J. B., Bahinski, A. and Izzo, N. J., Jr. (1998). HL-1 cells: a cardiac muscle cell line that contracts and retains phenotypic characteristics of the adult cardiomyocyte. Proc Natl Acad Sci U S A 95**,** 2979-84.

Di Pasquale, E., Song, B. and Condorelli, G. (2013). Generation of human cardiomyocytes: a differentiation protocol from feeder-free human induced pluripotent stem cells. *J Vis Exp*. 2013/07/16 ed.

Dobin, A., Davis, C. A., Schlesinger, F., Drenkow, J., Zaleski, C., Jha, S., Batut, P., Chaisson, M. and Gingeras, T. R. (2013). STAR: ultrafast universal RNA-seq aligner. Bioinformatics 29**,** 15-21.

Gu, Z. (2019). rGREAT: Client for GREAT Analysis.

Jawaid, W. (2019). enrichR: Provides an R Interface to 'Enrichr'. R package version 2.1 ed.

Kim, D., Paggi, J. M., Park, C., Bennett, C. and Salzberg, S. L. (2019). Graph-based genome alignment and genotyping with HISAT2 and HISAT-genotype. Nat Biotechnol 37**,** 907-915.

Kolde, R. (2019). pheatmap: Pretty Heatmaps. R package version 1.0.12 ed.

Kremer, K. and Grest, G. S. (1990). Dynamics of entangled linear polymer melts: A molecular-dynamics simulation. J Chem Phys 92**,** 5057-5086.

Kuleshov, M. V., Jones, M. R., Rouillard, A. D., Fernandez, N. F., Duan, Q., Wang, Z., Koplev, S., Jenkins, S. L., Jagodnik, K. M., Lachmann, A., et al. (2016). Enrichr: a comprehensive gene set enrichment analysis web server 2016 update. Nucleic Acids Res 44**,** W90-7.

Larcher, V., Kunderfranco, P., Vacchiano, M., Carullo, P., Erreni, M., Salamon, I., Colombo, F. S., Lugli, E., Mazzola, M., Anselmo, A., et al. (2018). An autofluorescence-based method for the isolation of highly purified ventricular cardiomyocytes. Cardiovasc Res 114**,** 409-416.

Li, H., Handsaker, B., Wysoker, A., Fennell, T., Ruan, J., Homer, N., Marth, G., Abecasis, G., Durbin, R. and Genome Project Data Processing, S. (2009). The Sequence Alignment/Map format and SAMtools. Bioinformatics 25**,** 2078-9.

Pertea, M., Pertea, G. M., Antonescu, C. M., Chang, T. C., Mendell, J. T. and Salzberg, S. L. (2015). StringTie enables improved reconstruction of a transcriptome from RNA-seq reads. Nat Biotechnol 33**,** 290-5.

Plimpton, S. (1995). Fast parallel algorithms for short-range molecular dynamics. J Comput Phys 117**,** 1-19.

Quinlan, A. R. and Hall, I. M. (2010). BEDTools: a flexible suite of utilities for comparing genomic features. Bioinformatics 26**,** 841-2.

R Core Team (2019). R: A language and environment for statistical computing. Vienna, Austria: R Foundation for Statistical Computing.

Robinson, M. D., Mccarthy, D. J. and Smyth, G. K. (2010). edgeR: a Bioconductor package for differential expression analysis of digital gene expression data. Bioinformatics 26**,** 139-40.

Salvarani, N., Crasto, S., Miragoli, M., Bertero, A., Paulis, M., Kunderfranco, P., Serio, S., Forni, A., Lucarelli, C., Dal Ferro, M., et al. (2019). The K219T-Lamin mutation induces conduction defects through epigenetic inhibition

of SCN5A in human cardiac laminopathy. Nat Commun 10**,** 2267.

Wang, L., Wang, S. and Li, W. (2012). RSeQC: quality control of RNA-seq experiments. Bioinformatics 28**,** 2184-5.

Yamazaki, T., Souquere, S., Chujo, T., Kobelke, S., Chong, Y. S., Fox, A. H., Bond, C. S., Nakagawa, S., Pierron, G. and Hirose, T. (2018). Functional Domains of NEAT1 Architectural lncRNA Induce Paraspeckle Assembly through Phase Separation. Mol Cell 70**,** 1038-1053 e7.